

First-order State Space Model for Lightweight Image Super-resolution

Yujie Zhu¹, Xinyi Zhang¹, Yekai Lu¹, Guang Yang^{1,2}, Faming Fang¹, Guixu Zhang^{1*}

¹School of Computer Science and Technology, East China Normal University, Shanghai, China

²IT Department, Guotai Junan Security, Shanghai, China

52205901006@stu.ecnu.edu.cn, 51265901099@stu.ecnu.edu.cn, 51255901081@stu.ecnu.edu.cn,

51215901104@stu.ecnu.edu.cn, fmfang@cs.ecnu.edu.cn, gxzhang@cs.ecnu.edu.cn

Abstract—State space models (SSMs), particularly Mamba, have shown promise in NLP tasks and are increasingly applied to vision tasks. However, most Mamba-based vision models focus on network architecture and scan paths, with little attention to the SSM module. In order to explore the potential of SSMs, we modified the calculation process of SSM without increasing the number of parameters to improve the performance on lightweight super-resolution tasks. In this paper, we introduce the First-order State Space Model (FSSM) to improve the original Mamba module, enhancing performance by incorporating token correlations. We apply a first-order hold condition in SSMs, derive the new discretized form, and analyzed cumulative error. Extensive experimental results demonstrate that FSSM improves the performance of MambaIR on five benchmark datasets without additionally increasing the number of parameters, and surpasses current lightweight SR methods, achieving state-of-the-art results.

Index Terms—ODE, state space model, lightweight image super-resolution, error analysis

I. INTRODUCTION

Single image super-resolution (SR) aims to reconstruct a high-resolution output image from a given low-resolution image and is a well-known problem in computer vision. The development of deep learning models has significantly improved SR performance in recent years. Among these models, CNNs and Transformers are now dominant. CNNs efficiently combine information from adjacent pixels, resulting in lower computation costs but limiting their ability to capture global image information due to their restricted receptive fields. In contrast, Transformers can handle long-range dependencies between pixels, expanding their receptive fields but increasing computation cost, especially at higher resolutions.

The size of the receptive field greatly influences the representation capability of neural networks. However, balancing low computation cost with a large receptive field is challenging. Recently, structured state-space sequence (S4) models [1], particularly Mamba [2], have provided a way to balance global receptive fields with manageable computational costs. Mamba's recursive state-space equations model long-range dependencies with linear complexity. Additionally, Hippo [3] and H3 [4] models enhance this capability, reducing the performance gap between SSMs and Transformers. Furthermore, the parallel scan

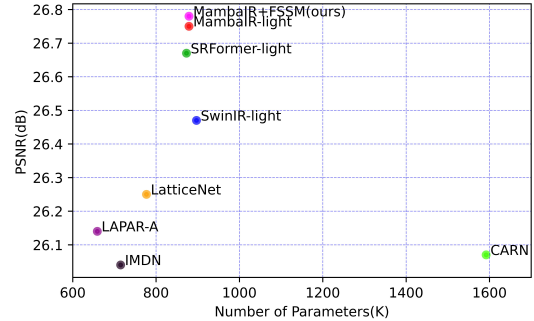


Fig. 1. Trade-off between the number of model parameters and performance on Urban100(x4).

algorithm [2], [5] accelerates the training process of Mamba by leveraging modern GPU capabilities.

Given Mamba's promising features, we introduce First-order State Space Model (FSSM), a first-order state-space model. FSSM is designed for tasks where the entire input sequence is available beforehand, enabling the use of correlations between adjacent tokens. To improve SSM module, we derive the discrete form with first-order hold condition. Besides, we analyzed the cumulative error and applied various expansion for better approximate. For enhanced computational efficiency, we also modify Mamba's CUDA code in our FSSM implementation.

Our main contributions can be summarized as follows:

- We propose First-order State Space Model (FSSM), which replaces traditional SSM module in Mamba block, improving its representation ability. Based on first-order hold condition, we re-derive discretization form of SSM.
- To balance the computational efficiency and precision, we applied multiple forms of approximation, and analyzed the cumulative error.
- We conduct experiments on light-weight SR by replacing SSM module with our FSSM module in MambaIR [6]. Fig. 1 provides a visual performance comparison, which demonstrate that our FSSM module improves the performance of MambaIR, and outperforms other strong baselines on light-weight image super-resolution task.

II. RELATED WORKS

A. Image Super-resolution

Image super-resolution has seen significant advancements since SRCNN [7] introduced deep convolutional neural

*Corresponding author

This work was supported by the National Key R&D Program of China (2022ZD0161800), and the National Natural Science Foundation of China under Grant 62271203.

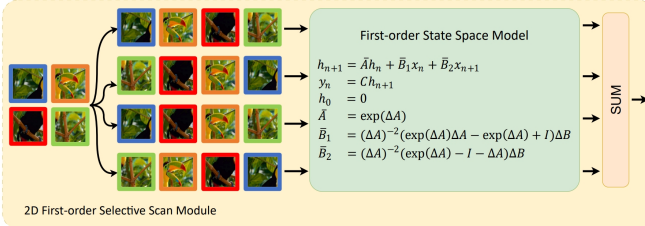


Fig. 2. The architecture diagram of 2D First-order Selective Scan Module.

networks (CNNs) to the task. Following SRCNN, various CNN blocks like residual [8], [9] and dense blocks [10], [11] have been developed to enhance model representation. However, CNN-based models struggle with capturing long-range and global dependencies effectively. On the other hand, Transformer-based models have shown strong results in SR tasks, setting new benchmarks recently. Transformers excel at capturing global information but face the challenge of quadratic computational complexity due to self-attention [12]. To mitigate this, some methods, like Swin-Transformer [12] and NAT [13], limit attention in neighboring patches or pixels. However, these approaches still face a trade-off between expanding the effective global receptive field and maintaining efficient attention computation which is a challenging issue in Transformer architecture.

B. State Space Model

Recently, the Structured State-Space Sequence (S4) model has emerged as a promising alternative to CNNs and Transformers due to its linear scaling with sequence length. The S5 layer [5], introduced with MIMO SSM and efficient parallel scanning, significantly accelerates training. H3 [4] further enhances the long-range dependency capability of SSMs, narrowing the performance gap with Transformers. More recently, Mamba [2], a data-dependent SSM, has outperformed Transformers in natural language processing while maintaining linear scaling. To adapt Mamba for vision tasks, various methods have been proposed, including the Cross-Scan Module [14] and bidirectional SSM with position embeddings [15]. Mamba has been applied to a variety of vision tasks, including image classification [14], [15], medical image segmentation [16], image generation [17], [18], image restoration [6], [19], video object segmentation [20] and others [21]–[23]. Our FSSM further enhances Mamba, improving it as a better backbone for super-resolution task.

III. METHOD

A. Overview of 2D First-order Selective Scan Module

We propose the 2D First-order Selective Scan Module for convenient plug-and-play. The architecture of our proposed module is shown in Fig. 2, aims to enhance the implicit expression ability to improve the effectiveness of SSM in lightweight SR tasks. The 2D First-order Selective Scan Module inputs the features into First-order State Space Model (FSSM) along four directions, and combined the results for output. Later we will describe the details of FSSM and analyze the cumulative error.

B. First-order State Space Model (FSSM)

The classical State Space Model (SSM) is generally considered to be a linear system

$$\begin{aligned} h'(t) &= A(t)h(t) + B(t)x(t) \\ y(t) &= C(t)h(t) \end{aligned} \quad (1)$$

that maps continuous input $x(t)$ to output $y(t)$ by introducing a state variable $h(t)$, where $x(t), y(t) \in C^0(\mathbb{R})$, $B(t), C(t) \in C^0(\mathbb{R}^D)$, and $A(t) \in C^0(\mathbb{R}^{D \times D})$. If the parameters of the system do not change over time t , it is referred to as a time-invariant SSM. For discrete data, we usually expand the discrete input $\{x_n\}$ to continuous $x(t)$, and then solve (1) to get the solution $y(t)$, finally taking time index of $y(t)$ to get discrete output $\{y_n\}$.

For time-invariant SSM, the general solutions of first-order linear ODEs on the interval $[t_n, t_{n+1}]$ can be solved as:

$$h(t) = e^{(t-t_n)A}h(t_n) + \int_{t_n}^t e^{(t-s)A}Bx(s)ds \quad (2)$$

where e^{xA} is matrix exponential function, defined as:

$$e^{xA} = I + xA + \frac{(xA)^2}{2!} + \dots + \frac{(xA)^k}{k!} + \dots \quad (3)$$

Noticed that traditional SSM usually expand $\{x_n\}$ with zero-order hold condition, which makes that only one-sided information can be used when extracting features by calculating SSM. In order to explore the potential of SSM in vision tasks, and to take full advantage of the relationship between the time steps, we try to improve the model based on the first-order hold condition, Fig. 3 compares the difference between the two extensions.

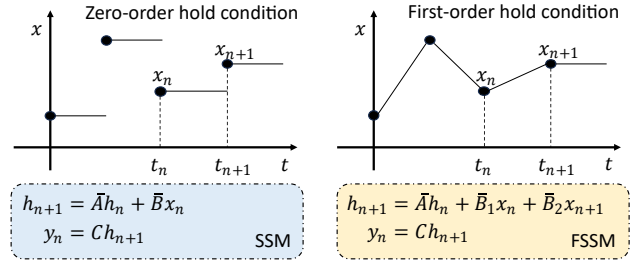


Fig. 3. SSM with different extensions.

Based on first-order hold condition, the formula of $x(t)$ over $[t_n, t_{n+1}]$ can be written by:

$$x(t) = x_n + \frac{t - t_n}{\Delta_n}(x_{n+1} - x_n) \quad (4)$$

where $\Delta_n = t_{n+1} - t_n$. Taking (4) into (2), we can get

$$\begin{aligned} h(t_{n+1}) &= e^{\Delta_n A}h(t_n) + \int_{t_n}^{t_{n+1}} e^{(t_{n+1}-s)A}Bx(s)ds \\ &= e^{\Delta_n A}h(t_n) \\ &\quad + (\Delta_n A)^{-2}(\Delta_n A e^{\Delta_n A} - e^{\Delta_n A} + I)\Delta_n Bx_n \\ &\quad + (\Delta_n A)^{-2}(e^{\Delta_n A} - I - \Delta_n A)\Delta_n Bx_{n+1} \end{aligned} \quad (5)$$

Finally, taking $h_n = h(t_n)$ and $h(0) = 0$, we get the discrete FSSM form

$$\begin{aligned} h_{n+1} &= \bar{A}h_n + \bar{B}_1x_n + \bar{B}_2x_{n+1} \\ y_n &= Ch_{n+1} \\ h_0 &= 0 \\ \bar{A} &= e^{\Delta_n A} \\ \bar{B}_1 &= (\Delta_n A)^{-2}(\Delta_n A e^{\Delta_n A} - e^{\Delta_n A} + I)\Delta_n B \\ \bar{B}_2 &= (\Delta_n A)^{-2}(e^{\Delta_n A} - I - \Delta_n A)\Delta_n B \end{aligned} \quad (6)$$

Similar to Mamba, we incorporate the selection mechanism into models by letting parameters (Δ, B, C) be time-dependent. We derive (Δ_n, B_n, C_n) from input x_n , and compute the discrete $\bar{A}, \bar{B}_1, \bar{B}_2$. Algorithm 1 provides the pseudo-code of FSSM pipeline.

Algorithm 1 First-order State Space Model (FSSM)

Input: $A, \{x_n\}$
Output: $\{y_n\}$

- 1: $h_0 = 0$
- 2: **while** $n \leq T$ **do**
- 3: $\Delta_n, B_n, C_n \leftarrow \text{linear}(x_n)$
- 4: $\bar{A} \leftarrow \text{discretize}(\Delta_n, A)$
- 5: **if** $n \leq T - 1$ **then**
- 6: $\bar{B}_1, \bar{B}_2 \leftarrow \text{discretize}(\Delta_n, B_n)$ %use (6)
- 7: $h_{n+1} = \bar{A}h_n + \bar{B}_1x_n + \bar{B}_2x_{n+1}$
- 8: **else**
- 9: $\bar{B} \leftarrow \text{discretize}(\Delta_n, B_n)$ %use Mamba [2] form
- 10: $h_{n+1} = \bar{A}h_n + \bar{B}x_n$
- 11: **end if**
- 12: $y_n = C_n h_{n+1}$
- 13: **end while**
- 14: **return** $\{y_n\}$

C. Approximation

Noticed that the discrete parameter \bar{B}_1, \bar{B}_2 has the inverse of ΔA , in order to avoid computing the inverse, we refine the approximation by using the series representation of matrix exponential function (3):

$$\bar{B}_1 = \frac{1}{2}\Delta_n B_n, \bar{B}_2 = \frac{1}{2}\Delta_n B_n \quad (7)$$

$$\bar{B}_1 = \left(\frac{1}{2} + \frac{1}{3}\Delta_n A\right)\Delta_n B_n, \bar{B}_2 = \left(\frac{1}{2} + \frac{1}{6}\Delta_n A\right)\Delta_n B_n \quad (8)$$

For higher precision, we tried two forms of approximation, and analyzed them with extensive experiments. We called form (7) FSSM and form (8) FSSM⁺.

D. Analysis

Since we only have discrete inputs $\{x_n\}$ instead of continuous $x(t)$, the missing part contributes to the accumulation of error in the output. Now we analyze the cumulative error of SSM and FSSM, in order to simplify the analysis, we disregard the selective mechanism and assume that (Δ, A, B, C) are time-independent. We consider $\{x_n\}$ are sampled from unknown real

$x(t), y(t)$ is solved with $x(t)$ by (1), and $\{y_n\}$ are calculated from SSM(or FSSM) with $\{x_n\}$.

a) **Theorem 1:** (Cumulative error of SSM). Consider discrete SSM form (Mamba [2]) with time-independent (Δ, A, B, C) . Assume $x(t) : \mathbb{R} \rightarrow \mathbb{R}$ is L-Lipschitz and satisfies $x(t_n) = x_n$. There exists $\xi \in (0, \Delta A)$, such that SSM satisfies

$$|y(t_n) - y_n| \leq CL|B|e^{\xi\Delta^2} \frac{e^{n\Delta A} - I}{e^{\Delta A} - I}. \quad (9)$$

b) **Theorem 2:** (Cumulative error of FSSM). Consider discrete FSSM form (6) with time-independent (Δ, A, B, C) . Assume $x(t) : \mathbb{R} \rightarrow \mathbb{R}$ is L-Lipschitz and satisfies $x(t_n) = x_n$. There exists $\xi \in (0, \Delta A)$, such that FSSM satisfies

$$|y(t_n) - y_n| \leq \frac{CL|B|e^{\xi\Delta^2}}{2} \frac{e^{n\Delta A} - I}{e^{\Delta A} - I}. \quad (10)$$

Noticed that FSSM has the same order of error as SSM, but has a lower upper bound of cumulative error.

IV. EXPERIMENTS

A. Datasets and Details

a) **Datasets and Evaluation:** We train our SR models on DIV2K [24] and DF2K(DIV2K + Flickr2K [9]) datasets. Following other SR works, we use Set5 [25], Set14 [26], B100 [27], Urban100 [28], and Manga109 [29] to evaluate the generalizability and effectiveness of different SR models. For quantitative metrics, we use PSNR and SSIM [30] scores calculated on the Y channel of the YCbCr space.

b) **Training Details:** According to previous works of SR [6], [31], [32], we perform data augmentation by applying horizontal flips and random rotations of 90°, 180°, and 270°, as well as cropping the original images into 64×64 patches. For network and training process, we choose identical network architecture and training settings with MambaIR. Additionally, we use pretrained weights from MambaIR as an initialization of corresponding upscaling ratio. Our model is trained with 4 NVIDIA 3090 GPUs.

B. Experiment results

We compare our MambaIR + FSSM⁺ (FMambaIR) model with several other state-of-the-art light-weight SR methods, including CARN [33], IMDN [34], LAPAR-A [35], LatticeNet [36], SwinIR-light [32], SRFFormer-light [37] and MambaIR-light [6]. Table I demonstrates that our proposed FMambaIR outperforms other methods almost on all five benchmark datasets and all scales. Specifically, our FMambaIR model surpasses original MambaIR by up to 0.24dB PSNR on the x2 scale Urban100 dataset with the same network architecture and amount of parameters. Meanwhile, visual results comparison is provided in Fig 4. We observe that our model recover images more accurately while other approaches introduce some obvious structural distortions into recovered results.

TABLE I
QUANTITATIVE COMPARISON WITH STATE-OF-THE-ART METHODS ON BENCHMARK DATASETS. THE BEST RESULTS ARE HIGHLIGHTED IN BLACK BOLD AND THE SECOND BEST IS IN UNDERLINE.

Method	Scale	Params	Training Dataset	Set5		Set14		B100		Urban100		Manga109	
				PSNR / SSIM	PSNR / SSIM	PSNR / SSIM	PSNR / SSIM	PSNR / SSIM	PSNR / SSIM				
CARN [33]	x2	1,592K	DIV2K	37.76 / 0.9590	33.52 / 0.9166	32.09 / 0.8978	31.92 / 0.9256	38.36 / 0.9765					
IMDN [34]		694K	DIV2K	38.00 / 0.9605	33.63 / 0.9177	32.19 / 0.8996	32.17 / 0.9283	38.88 / 0.9774					
LAPAR-A [35]		548K	DF2K	38.01 / 0.9605	33.62 / 0.9183	32.19 / 0.8999	32.10 / 0.9283	38.67 / 0.9772					
LatticeNet [36]		756K	DIV2K	38.15 / 0.9610	33.78 / 0.9193	32.25 / 0.9005	32.43 / 0.9302	- / -					
SwinIR-light [32]		878K	DIV2K	38.14 / 0.9611	33.86 / 0.9206	32.31 / 0.9012	32.76 / 0.9340	39.12 / 0.9783					
SRFormer-light [37]		853K	DIV2K	38.23 / 0.9613	33.94 / 0.9209	32.36 / 0.9019	32.91 / 0.9353	39.28 / 0.9785					
MambaR-light [6]		859K	DIV2K	38.16 / 0.9610	34.00 / 0.9212	32.34 / 0.9017	32.92 / 0.9356	39.31 / 0.9779					
FMambaR(ours)		859K	DIV2K	38.20 / 0.9616	34.12 / 0.9225	32.37 / 0.9029	33.16 / 0.9372	39.43 / 0.9788					
FMambaR(ours)		859K	DF2K	38.25 / 0.9618	34.21 / 0.9230	32.41 / 0.9033	33.29 / 0.9381	39.59 / 0.9792					
CARN [33]	x3	1,592K	DIV2K	34.29 / 0.9255	30.29 / 0.8407	29.06 / 0.8034	28.06 / 0.8493	33.50 / 0.9440					
IMDN [34]		703K	DIV2K	34.36 / 0.9270	30.32 / 0.8417	29.09 / 0.8046	28.17 / 0.8519	33.61 / 0.9445					
LAPAR-A [35]		544K	DF2K	34.36 / 0.9267	30.34 / 0.8421	29.11 / 0.8054	28.15 / 0.8523	33.51 / 0.9441					
LatticeNet [36]		765K	DIV2K	34.53 / 0.9281	30.39 / 0.8424	29.15 / 0.8059	28.33 / 0.8538	- / -					
SwinIR-light [32]		886K	DIV2K	34.62 / 0.9289	30.54 / 0.8463	29.20 / 0.8082	28.66 / 0.8624	33.98 / 0.9478					
SRFormer-light [37]		861K	DIV2K	34.67 / 0.9296	30.57 / 0.8469	29.26 / 0.8099	28.81 / 0.8655	34.19 / 0.9489					
MambaR-light [6]		867K	DIV2K	34.72 / 0.9296	30.63 / 0.8475	29.29 / 0.8099	29.00 / 0.8689	34.39 / 0.9495					
FMambaR(ours)		867K	DIV2K	34.73 / 0.9301	30.63 / 0.8482	29.31 / 0.8119	29.02 / 0.8690	34.39 / 0.9497					
FMambaR(ours)		867K	DF2K	34.78 / 0.9304	30.65 / 0.8487	29.33 / 0.8124	29.13 / 0.8712	34.65 / 0.9505					
CARN [33]	x4	1,592K	DIV2K	32.13 / 0.8937	28.60 / 0.7806	27.58 / 0.7349	26.07 / 0.7837	30.47 / 0.9084					
IMDN [34]		715K	DIV2K	32.21 / 0.8948	28.58 / 0.7811	27.56 / 0.7353	26.04 / 0.7838	30.45 / 0.9075					
LAPAR-A [35]		659K	DF2K	32.15 / 0.8944	28.61 / 0.7818	27.61 / 0.7366	26.14 / 0.7871	30.42 / 0.9074					
LatticeNet [36]		777K	DIV2K	32.30 / 0.8962	28.68 / 0.7830	27.62 / 0.7367	26.25 / 0.7873	- / -					
SwinIR-light [32]		897K	DIV2K	32.44 / 0.8976	28.77 / 0.7858	27.69 / 0.7406	26.47 / 0.7980	30.92 / 0.9151					
SRFormer-light [37]		873K	DIV2K	32.51 / 0.8988	28.82 / 0.7872	27.73 / 0.7422	26.67 / 0.8032	31.17 / 0.9165					
MambaR-light [6]		879K	DIV2K	32.51 / 0.8993	28.85 / 0.7876	27.75 / 0.7423	26.75 / 0.8051	31.26 / 0.9175					
FMambaR(ours)		879K	DIV2K	32.51 / 0.9000	28.83 / 0.7878	27.77 / 0.7448	26.78 / 0.8053	31.16 / 0.9169					
FMambaR(ours)		879K	DF2K	32.56 / 0.9002	28.94 / 0.7896	27.80 / 0.7457	26.83 / 0.8076	31.42 / 0.9187					

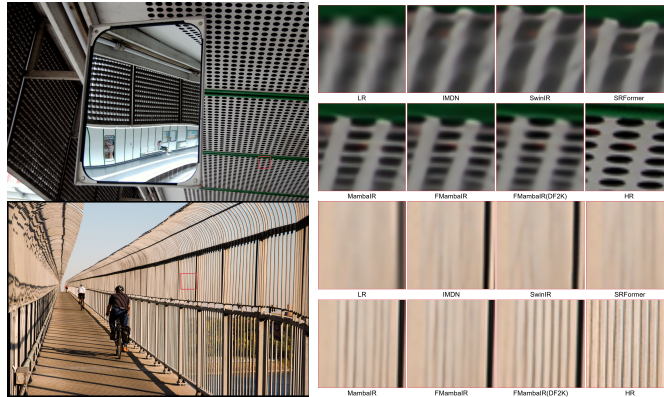


Fig. 4. Qualitative Comparison of our FMambaIR model with SOTA lightweight SR models on x4 upscaling task.

C. Ablation Study

a) *Effects of different extensions:* Expand condition is the core component of SSM. Using higher-order expand condition can improve the correlation between the tokens, and reduce the cumulative error. In this section, we ablate different extensions of SSM. In Table I we compared SSM and FSSM⁺ module trained under dataset DIV2K, for more comparative experiments, we also trained two methods under DF2K dataset. The PSNR and SSIM results of x2, x3, x4 light-weight SR presented in Table II show that FSSM⁺ module can enhance the performance since we take the correlation between tokens into account.

b) *Effects of different discretization approximation:* Increasing the expansion order can reduce the truncation error, and thus reduce the cumulative error. In this section, we compare different expansion order of approximation, FSSM (7) and FSSM⁺ (8) on benchmark datasets. The PSNR results

TABLE II
EFFECTS OF DIFFERENT EXTENSIONS OF SSM ON BENCHMARK DATASETS.

Module	Scale	Set5		Set14		B100		Urban100		Manga109	
		PSNR / SSIM	PSNR / SSIM	PSNR / SSIM	PSNR / SSIM	PSNR / SSIM	PSNR / SSIM				
SSM	x2	38.23 / 0.9618	34.17 / 0.9226	32.38 / 0.9030	33.19 / 0.9377	39.49 / 0.9789					
FSSM ⁺		38.25 / 0.9618	34.21 / 0.9230	32.41 / 0.9033	33.29 / 0.9381	39.59 / 0.9792					
SSM	x3	34.76 / 0.9302	30.65 / 0.8484	29.33 / 0.8123	29.09 / 0.8701	34.51 / 0.9500					
FSSM ⁺		34.78 / 0.9304	30.65 / 0.8487	29.33 / 0.8124	29.13 / 0.8712	34.65 / 0.9505					
SSM	x4	32.54 / 0.9000	28.92 / 0.7893	27.78 / 0.7450	26.82 / 0.8074	31.38 / 0.9184					
FSSM ⁺		32.56 / 0.9002	28.94 / 0.7896	27.80 / 0.7457	26.83 / 0.8076	31.42 / 0.9187					

of x2, x3, x4 light-weight SR presented in Table III show that more expansion terms can improve the performance. Note that with higher expansion, the remainder contains less valid information, so the improvement becomes smaller.

V. CONCLUSION

In this paper, we propose the First-order State Space Model (FSSM) to enhance the fundamental SSM module in Mamba architecture. We derive a new discretization form based on the first-order hold condition, use higher approximation to enhance the computational precision and analyze the cumulative error. Experiments show that FSSM improves the basic Mamba module and outperforms state-of-the-art methods in lightweight super-resolution. Given its promising results compared to vanilla Mamba, we are excited about FSSM's potential across various tasks and domains.

REFERENCES

[1] A. Gu, K. Goel, and C. Ré, “Efficiently modeling long sequences with structured state spaces,” *arXiv preprint arXiv:2111.00396*, 2021.

[2] A. Gu and T. Dao, “Mamba: Linear-time sequence modeling with selective state spaces,” *arXiv preprint arXiv:2312.00752*, 2023.

[3] A. Gu, T. Dao, S. Ermon, A. Rudra, and C. Ré, “Hippo: Recurrent memory with optimal polynomial projections,” *Advances in neural information processing systems*, vol. 33, pp. 1474–1487, 2020.

[4] D. Y. Fu, T. Dao, K. K. Saab, A. W. Thomas, A. Rudra, and C. Ré, “Hungry hungry hippos: Towards language modeling with state space models,” *arXiv preprint arXiv:2212.14052*, 2022.

[5] J. T. Smith, A. Warrington, and S. W. Linderman, “Simplified state space layers for sequence modeling,” *arXiv preprint arXiv:2208.04933*, 2022.

[6] H. Guo, J. Li, T. Dai, Z. Ouyang, X. Ren, and S.-T. Xia, “Mambair: A simple baseline for image restoration with state-space model,” *arXiv preprint arXiv:2402.15648*, 2024.

[7] C. Dong, C. C. Loy, K. He, and X. Tang, “Learning a deep convolutional network for image super-resolution,” in *Computer Vision–ECCV 2014: 13th European Conference, Zurich, Switzerland, September 6–12, 2014, Proceedings, Part IV 13*. Springer, 2014, pp. 184–199.

[8] J. Kim, J. K. Lee, and K. M. Lee, “Accurate image super-resolution using very deep convolutional networks,” in *Proceedings of the IEEE conference on computer vision and pattern recognition*, 2016, pp. 1646–1654.

[9] B. Lim, S. Son, H. Kim, S. Nah, and K. Mu Lee, “Enhanced deep residual networks for single image super-resolution,” in *Proceedings of the IEEE conference on computer vision and pattern recognition workshops*, 2017, pp. 136–144.

[10] X. Wang, K. Yu, S. Wu, J. Gu, Y. Liu, C. Dong, Y. Qiao, and C. Change Loy, “EsrGAN: Enhanced super-resolution generative adversarial networks,” in *Proceedings of the European conference on computer vision (ECCV) workshops*, 2018, pp. 0–0.

[11] Y. Zhang, Y. Tian, Y. Kong, B. Zhong, and Y. Fu, “Residual dense network for image super-resolution,” in *Proceedings of the IEEE conference on computer vision and pattern recognition*, 2018, pp. 2472–2481.

[12] Z. Liu, Y. Lin, Y. Cao, H. Hu, Y. Wei, Z. Zhang, S. Lin, and B. Guo, “Swin transformer: Hierarchical vision transformer using shifted windows,” in *Proceedings of the IEEE/CVF international conference on computer vision*, 2021, pp. 10012–10022.

[13] A. Hassani, S. Walton, J. Li, S. Li, and H. Shi, “Neighborhood attention transformer,” in *Proceedings of the IEEE/CVF Conference on Computer Vision and Pattern Recognition*, 2023, pp. 6185–6194.

[14] Y. Liu, Y. Tian, Y. Zhao, H. Yu, L. Xie, Y. Wang, Q. Ye, and Y. Liu, “Vmamba: Visual state space model,” *arXiv preprint arXiv:2401.10166*, 2024.

[15] L. Zhu, B. Liao, Q. Zhang, X. Wang, W. Liu, and X. Wang, “Vision mamba: Efficient visual representation learning with bidirectional state space model,” *arXiv preprint arXiv:2401.09417*, 2024.

[16] J. Ma, F. Li, and B. Wang, “U-mamba: Enhancing long-range dependency for biomedical image segmentation,” *arXiv preprint arXiv:2401.04722*, 2024.

[17] L. Fu, X. Li, X. Cai, Y. Wang, X. Wang, Y. Shen, and Y. Yao, “Md-dose: A diffusion model based on the mamba for radiotherapy dose prediction,” *arXiv preprint arXiv:2403.08479*, 2024.

[18] V. T. Hu, S. A. Baumann, M. Gui, O. Grebenkova, P. Ma, J. Fischer, and B. Ommer, “Zigma: Zigzag mamba diffusion model,” *arXiv preprint arXiv:2403.13802*, 2024.

[19] Z. Zheng and C. Wu, “U-shaped vision mamba for single image dehazing,” *arXiv preprint arXiv:2402.04139*, 2024.

[20] Y. Yang, Z. Xing, and L. Zhu, “Vivim: a video vision mamba for medical video object segmentation,” *arXiv preprint arXiv:2401.14168*, 2024.

[21] E. Nguyen, K. Goel, A. Gu, G. Downs, P. Shah, T. Dao, S. Baccus, and C. Ré, “S4nd: Modeling images and videos as multidimensional signals with state spaces,” *Advances in neural information processing systems*, vol. 35, pp. 2846–2861, 2022.

[22] M. M. Islam, M. Hasan, K. S. Athrey, T. Braskich, and G. Bertasius, “Efficient movie scene detection using state-space transformers,” in *Proceedings of the IEEE/CVF Conference on Computer Vision and Pattern Recognition*, 2023, pp. 18749–18758.

[23] D. Liang, X. Zhou, X. Wang, X. Zhu, W. Xu, Z. Zou, X. Ye, and X. Bai, “Pointmamba: A simple state space model for point cloud analysis,” *arXiv preprint arXiv:2402.10739*, 2024.

[24] E. Agustsson and R. Timofte, “Ntire 2017 challenge on single image super-resolution: Dataset and study,” in *Proceedings of the IEEE conference on computer vision and pattern recognition workshops*, 2017, pp. 126–135.

[25] M. Bevilacqua, A. Roumy, C. Guillemot, and M. L. Alberi-Morel, “Low-complexity single-image super-resolution based on nonnegative neighbor embedding,” 2012.

[26] R. Zeyde, M. Elad, and M. Protter, “On single image scale-up using sparse-representations,” in *Curves and Surfaces: 7th International Conference, Avignon, France, June 24–30, 2010, Revised Selected Papers 7*. Springer, 2012, pp. 711–730.

[27] D. Martin, C. Fowlkes, D. Tal, and J. Malik, “A database of human segmented natural images and its application to evaluating segmentation algorithms and measuring ecological statistics,” in *Proceedings Eighth IEEE International Conference on Computer Vision. ICCV 2001*, vol. 2. IEEE, 2001, pp. 416–423.

[28] J.-B. Huang, A. Singh, and N. Ahuja, “Single image super-resolution from transformed self-exemplars,” in *Proceedings of the IEEE conference on computer vision and pattern recognition*, 2015, pp. 5197–5206.

[29] Y. Matsui, K. Ito, Y. Aramaki, A. Fujimoto, T. Ogawa, T. Yamasaki, and K. Aizawa, “Sketch-based manga retrieval using manga109 dataset,” *Multimedia tools and applications*, vol. 76, pp. 21811–21838, 2017.

[30] Z. Wang, A. C. Bovik, H. R. Sheikh, and E. P. Simoncelli, “Image quality assessment: from error visibility to structural similarity,” *IEEE transactions on image processing*, vol. 13, no. 4, pp. 600–612, 2004.

[31] X. Chen, X. Wang, J. Zhou, Y. Qiao, and C. Dong, “Activating more pixels in image super-resolution transformer,” in *Proceedings of the IEEE/CVF conference on computer vision and pattern recognition*, 2023, pp. 22367–22377.

[32] J. Liang, J. Cao, G. Sun, K. Zhang, L. Van Gool, and R. Timofte, “Swinir: Image restoration using swin transformer,” in *Proceedings of the IEEE/CVF international conference on computer vision*, 2021, pp. 1833–1844.

[33] N. Ahn, B. Kang, and K.-A. Sohn, “Fast, accurate, and lightweight super-resolution with cascading residual network,” in *Proceedings of the European conference on computer vision (ECCV)*, 2018, pp. 252–268.

[34] Z. Hui, X. Gao, Y. Yang, and X. Wang, “Lightweight image super-resolution with information multi-distillation network,” in *Proceedings of the 27th ACM international conference on multimedia*, 2019, pp. 2024–2032.

[35] W. Li, K. Zhou, L. Qi, N. Jiang, J. Lu, and J. Jia, “Lapar: Linearly-assembled pixel-adaptive regression network for single image super-resolution and beyond,” *Advances in Neural Information Processing Systems*, vol. 33, pp. 20343–20355, 2020.

[36] X. Luo, Y. Xie, Y. Zhang, Y. Qu, C. Li, and Y. Fu, “Latticenet: Towards lightweight image super-resolution with lattice block,” in *Computer Vision–ECCV 2020: 16th European Conference, Glasgow, UK, August 23–28, 2020, Proceedings, Part XXII 16*. Springer, 2020, pp. 272–289.

[37] Y. Zhou, Z. Li, C.-L. Guo, S. Bai, M.-M. Cheng, and Q. Hou, “Srformer: Permutated self-attention for single image super-resolution,” in *Proceedings of the IEEE/CVF International Conference on Computer Vision*, 2023, pp. 12780–12791.